

2013

# Fault Dating in Rosendale, New York Using Clay Polytype Quantification

Patrick S. Donohue

Follow this and additional works at: [http://digitalwindow.vassar.edu/senior\\_capstone](http://digitalwindow.vassar.edu/senior_capstone)

---

## Recommended Citation

Donohue, Patrick S., "Fault Dating in Rosendale, New York Using Clay Polytype Quantification" (2013). *Senior Capstone Projects*. 233.  
[http://digitalwindow.vassar.edu/senior\\_capstone/233](http://digitalwindow.vassar.edu/senior_capstone/233)

This Open Access is brought to you for free and open access by Digital Window @ Vassar. It has been accepted for inclusion in Senior Capstone Projects by an authorized administrator of Digital Window @ Vassar. For more information, please contact [library\\_thesis@vassar.edu](mailto:library_thesis@vassar.edu).

# Fault Dating in Rosendale, New York Using Clay Polytype Quantification

Patrick S. Donohue

May 2013

Undergraduate Thesis

Vassar College Department of Earth Science, Poughkeepsie NY

---

Advised by Professor Jeff Walker

## Table of Contents

Abstract	3
Introduction	4
Methods	13
Results	18
Results (Figures)	21
Discussion	26
Bibliography	29

## Abstract

The techniques of fault dating, though still underdeveloped on a wide scale, have been increasingly studied over the past decade. This study draws on these recent observations in relative literature and relates them to a fault in Rosendale, New York, the location of significant tectonic events during the mid to late Paleozoic. Direct dating of clay-rich brittle fault gouges involves two components: clay polytype quantification and  $^{40}\text{Ar}/^{39}\text{Ar}$  thermochronological dating. This study will focus on the polytype quantification aspect of the dating process. Polytypes are variations in mineral structure which can be related to the conditions of formation of the clay mineral. The two polytypes of illite formed in a fault are  $2\text{M}_1$ , reflecting the detrital material from the wall rock of the fault, and  $1\text{M}/1\text{M}_d$  which are authigenic clays that form during movement on the fault. By splitting the fault gouge sample into three grain size fractions and determining the percentages of each polytype in each fraction, we can project the age of the fault. We used X-ray diffraction analysis to measure polytype peak intensities and WILDFIRE© modeling software to determine percentages. Our results showed that the largest size fraction's comparative polytype percentage was 33.33%  $1\text{M}$  and 66.66%  $2\text{M}_1$ , the intermediate size fraction's comparative percentage was 50%  $1\text{M}$  and 50%  $2\text{M}_1$ , and the smallest size fraction's comparative percentage was 77.77%  $1\text{M}$  and 22.22%  $2\text{M}_1$ . The percentages of the three size fractions can be graphed against the  $^{40}\text{Ar}/^{39}\text{Ar}$  age and extrapolated until pure authigenic age is determined. This step will be carried out by our colleagues at the University of Michigan.

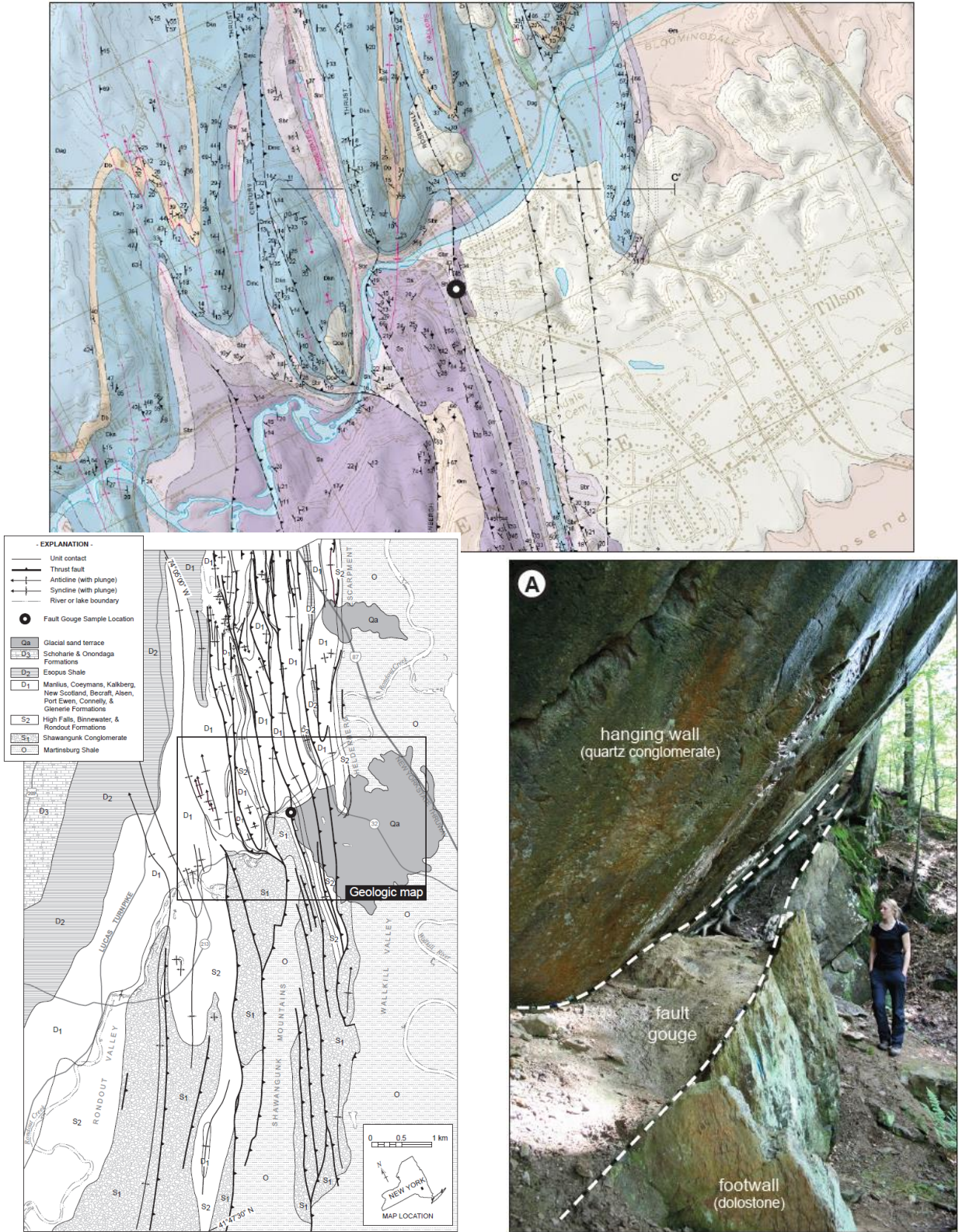
## Introduction

The Hudson River Valley of New York underwent extreme tectonic compression during several intervals in the Paleozoic Era and was effected by major tectonic events on North America's eastern seaboard for hundreds of millions of years prior to the Paleozoic (Budnik et al., 2010). The most important Paleozoic convergent events include the Taconic Orogeny, approximately 450 million years ago, caused by the collision of the Taconic Island Chain with Proto-North America, the Acadian Orogeny, caused when the Avalonian Island Arc struck around 375 million years ago, and the Alleghanian Orogeny, caused when the Proto-African continent struck around 260 million years ago (Burmeister and Marshak, 2006). The Acadian Orogeny is sometimes included as part of the Taconic Orogeny. The orogenies resulted from the early stages of the formation of Pangaea. Around 200 million years ago, Pangaea began to split apart. The rift is still expanding today at the Mid-Atlantic Ridge. Since that time, the coast of North America, and thus the entire state of New York, has been on a passive margin (Budnik et al., 2010).

Within the Hudson Valley, a fold-thrust belt involving Late Silurian to Middle Devonian strata outcrops from Catskill through Kingston to Rosendale. Along the belt, Ordovician flysch sequences, deposited while the area was a shallow sea, dominate the lowest level of stratigraphy. Flysch is a sedimentary sequence deposited in marine conditions, typically found in tectonically convergent areas. It is indicative of a deepening foreland basin which is penned in by an island arc. As the island arc moves towards the coast and the continental plate, the foreland basin deepens, causing a change in sedimentary deposition. The sedimentary sequence begins with sandstones while the basin is shallow and higher energy. As the island arc moves in, the

depositional area is moved offshore and shales and greywackes are deposited. In this situation, the flysch is a turbidite, meaning it was deposited by a density flow. Directly above these turbidites lies the Taconic unconformity, caused by the tectonic activity of the Taconic Orogeny. Near Rosendale, above the unconformity lies a collection of Late Silurian clastic and carbonate layers including the Shawangunk conglomerate, the High Falls shale, the Binnewater sandstone, and the Rondout Formation (sandy limestones). A gradual movement from a high energy shoreline environment (conglomerates, sandstones) to a lower energy deep sea environment (shales, limestones) represents a deepening foreland basin. Above those lie a series of limestone groups overlain by the weak Esopus shale. Near Rosendale, the Esopus is ultimately capped by limestone of the Schoharie Formation. These limestones and shales reinforce the idea of a lower energy deep sea environment (Burmeister and Marshak, 2006).

The thrust fault whose gouge was sampled is found just outside the village of Rosendale (Figs. 1 and 2). It is just south of the Rondout Creek on the northwestern side of the Shawangunk Mountains. It is surrounded by a number of thrust faults (north-south lines in Fig. 1), none of which have been dated. It is thought that these faults were caused by either the Acadian or the Alleghanian Orogenies, so they were formed between 375 and 260 million years ago (Burmeister and Marshak, 2006). This particular fault gouge shears through a dolostone footwall and a quartz conglomerate hanging wall, (Fig. 3). The dolostone is from either the Whiteport or Rosendale members of the Rondout Formation. The quartz conglomerate could be from a wider variety of formations, but the Shawangunk Formation's quartz conglomerate is a likely source (Burmeister and Marshak, 2006).



**Figs. 1 and 2 (left, top):** Geologic map and inset of the fault gouge sample location (black circle) and local Rosendale geology.

**Figure 3 (right):** Photograph of the sampling site and its fault geology.

The fault gouge itself is the result of the two sides of the fault grinding each other into fine fragments through tectonic forces. A fault gouge is primarily shale-rich and is characterized by a small grain size. Clasts in a fault gouge are loosely assorted with little to no cohesion, making it easy for sample collection. The loose nature of a fault gouge causes discontinuity of lithification which results in a lack of structural integrity.

The dating of previously undated faults has multiple uses in today's science. Dating these faults is central in the discussion of mountain building and its effects on climate. To gain a more precise knowledge of our planet's current and future climate, it is imperative that we understand past climates and the different forces that affect that climate. Tectonics is becoming noted as a major actor in climate change (Rahl et al., 2011). Additionally, knowing the date of a fault can offer insight into the tectonic event that caused it and contribute to the understanding of local topography, past and present. Such knowledge of timescales can be applied to areas with similar geologic formations to help better imagine past events. An integral application of this idea is determining the erosional rates of mountains and how they relate to crustal deformation (Rahl et al., 2011).

It is difficult, however, to use typical dating measures to find the age of fault gouges since the local stratigraphic units are often disrupted or muddled. Recently, isotopic dating of clays has provided the alternative necessary to date faults (Pevear, 1998; Duvall et al., 2011). To accurately use this medium, we turn to clay mineralogy and X-ray diffraction techniques. The fault gouge has many components and XRD is necessary to distinguish those components.

Clay mineral structures are made up by two main structural units; tetrahedral sheets and octahedral sheets. A tetrahedron is made up of four oxygen atoms in tetrahedral coordination

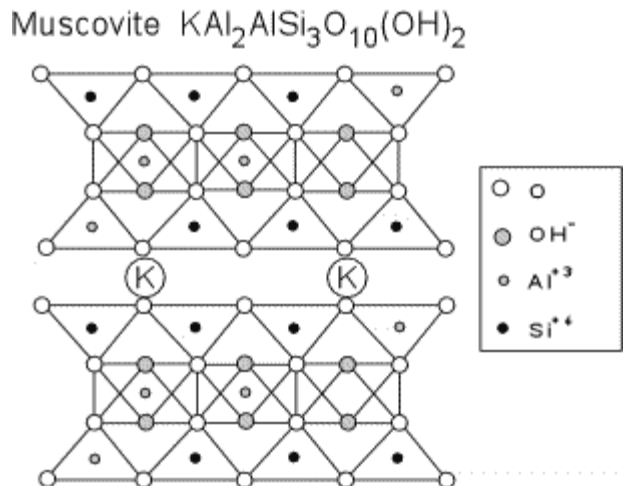


**Figure 4:** Example of the TOT structure of clays (Moore and Reynolds, 1997).

tetrahedral (or TOT) sheets in which oxygen molecules from the tetrahedral sheets replace four of the OH molecules from the octahedral structure.

These layers are then bonded to adjacent layers in several ways: with weak Van der Waals bonds (found in talc), with hydrogen bonds (found in serpentine), with an octahedral sheet of OH coordinated around a Mg atom (found in chlorite), and with coordination around a cation (ex:  $K^+$ ) that fits in the hexagonal holes of adjacent TOT layers (found in illite) (Moore and Reynolds, 1997). A diagram of the TOT structure in illite can be found in Figure 4. The clay mineral found in the Rosendale fault gouge is illite, “a general term for dioctahedral mica-like clay common in sedimentary rocks, especially shales” (Pevear, 1999). The  $K^+$  in the layer cation in illite is easily leached, allowing weathering to disrupt its composition. The process of weathering gives calcium cations an avenue through which to replace the  $K^+$ . This chemical replacement creates a different mineral, smectite, which is much younger than the illite from which it is formed. Because weathering affects the  $K^+$  cations important for  $^{40}Ar/^{39}Ar$  dating, the sample to be dated must be as unweathered as possible.

around a silicon or an aluminum atom. These tetrahedra are connected and arranged in sheets of hexagonal symmetry having a chemical formula of  $Si_4O_{10}$ . An octahedra, on the other hand, consists of six O or OH molecules in octahedral coordination about an aluminum or magnesium atom. The basic clay structure is a layer with alternating tetrahedral-octahedral-

Clay mineral structures allow for a significant amount of structural differentiation in addition to the interlayer differences discussed above. Layered silicates such as illite also can contain several structural arrangements, known as polytypes. The structural arrangement is formed by the orientation of the TOT layers, and a process has been developed to date these clay samples by observing and analyzing the different orientations. Viewed from the top, the TOT layers have hexagonal symmetry. The alignment of the hexagonal sheets in successive layers rotates with the potassium atom used as a standard point (as represented by the filled circle symbols in Fig. 1A). The most common polytypes of clay are monoclinic, classified with a capital M. Monoclinic shifts in polytypes are characterized by two perpendicular axes and one

oblique angle (the  $\beta$ -angle, between the X and Z planes). This  $\beta$  angle defines the orientation of the layer, so when subsequent layers “rotate,” in actuality the orientation of the  $\beta$  angle is what is rotating. A monoclinic stacking with no rotation is referred to as 1M. Monoclinic stacking with alternating TOT sheet rotation is referred to as  $2M_1$  (Moore and Reynolds, 1997). A disordered monoclinic polytype,  $1M_d$ , has random 60 or 120 degree monoclinic rotations (Haines and van der Pluijm, 2008). Another illite polytype is trigonal rather than monoclinic, referred to as 3T (Figure 5), though it is not common in sedimentary rocks.

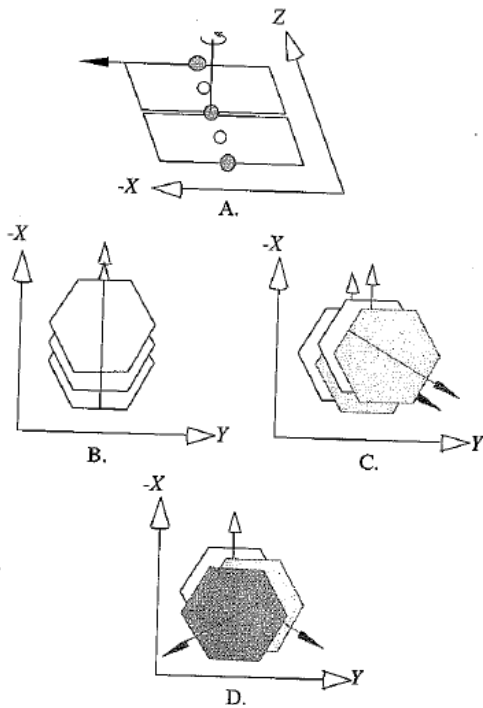


**Figure 5:** Examples of monoclinic illite polytypes. A: X-Y plane layer rotation. B: 1M stacking. C: 2M stacking. D: 3T full rotational stacking (Moore and Reynolds 1997).

Clay polytypes are the key to determining the age of fault gouges. The clay particles in a fault gouge could be either detrital (weathered and transported to the site) or authigenic (clay crystals grown within the site during faulting). It is assumed that  $2M_1$  polytypes are detrital while  $1M$  and  $1M_d$  polytypes are authigenic (Duvall et. al, 2011; Haines and van der Pluijm, 2008; Pevear, 1999; Rahl et. al., 2011). By using different clay size fractions and their relative ratios of polytypes the age of the authigenic illite can be determined (Duvall et. al., 2011). It is also important to note that if the fault has undergone multiple events, the illite analysis would only be a viable representation for the most recent fault activity or the age of the authigenic formation of the clay in the fault (Duvall et. al., 2011).

Temperature is an important variable for illite growth. It is currently thought that  $2M_1$  illite polytypes form at above  $280^\circ\text{C}$  and  $1M$  and  $1M_d$  illite polytypes form below  $200^\circ\text{C}$  (Duvall et al., 2011). The  $<200^\circ\text{C}$  formation temperature for authigenic illite implies that it formed in the brittle deformation realm (Haines and van der Pluijm, 2008). The range of temperature at which the illite could have formed is restricted, which restricts the possible depths at which the fault formed. This suggests a correlation between depth and age of the fault, offering insight about the nature of the area at the time of the fault activity (Duvall et. al., 2008).

The ratio of polytypes in the fault gouge clays is determined using X-ray diffraction (XRD). Diffraction occurs when X-rays strike a mineral sample, and are reflected at particular angles based on the spacing and atomic planes in the minerals present (Fig. 6). The detector records the number of X-rays or “intensity” at each diffraction angle. Intensity is graphed against the  $2\theta$  angle at which it was recorded (Fig. 6). The pattern of the peaks correlates to different mineral structures. To identify a mineral, a formula which is a function of the diffraction angle

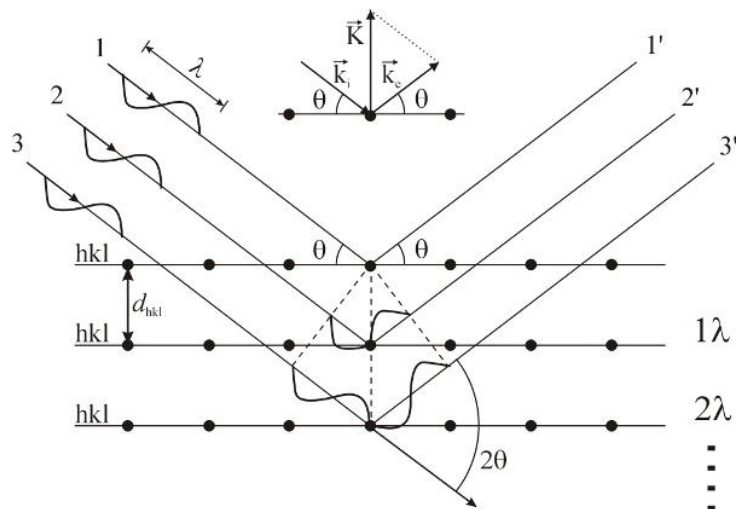


**Figure 6:** A graphical representation of 2Theta, d, and clay structure in XRD format.

and the position and identity of the atoms in the crystal calculates the distance ( $d$  – Fig. 6) between equivalent points between two unit cells. That distance ( $d$ ) at each  $2\theta$  angle can be correlated to a specific mineral structure (Haines and van der Pluijm, 2008; Rahl et. al, 2011), as shown in Fig. 7. In order to fully

analyze the XRD results, WILDFIRE© modeling software is used to identify the ratio of different polytypes by mixing and adding together different XRD patterns (Haines and van der Pluijm, 2008; Duvall et. al., 2011).

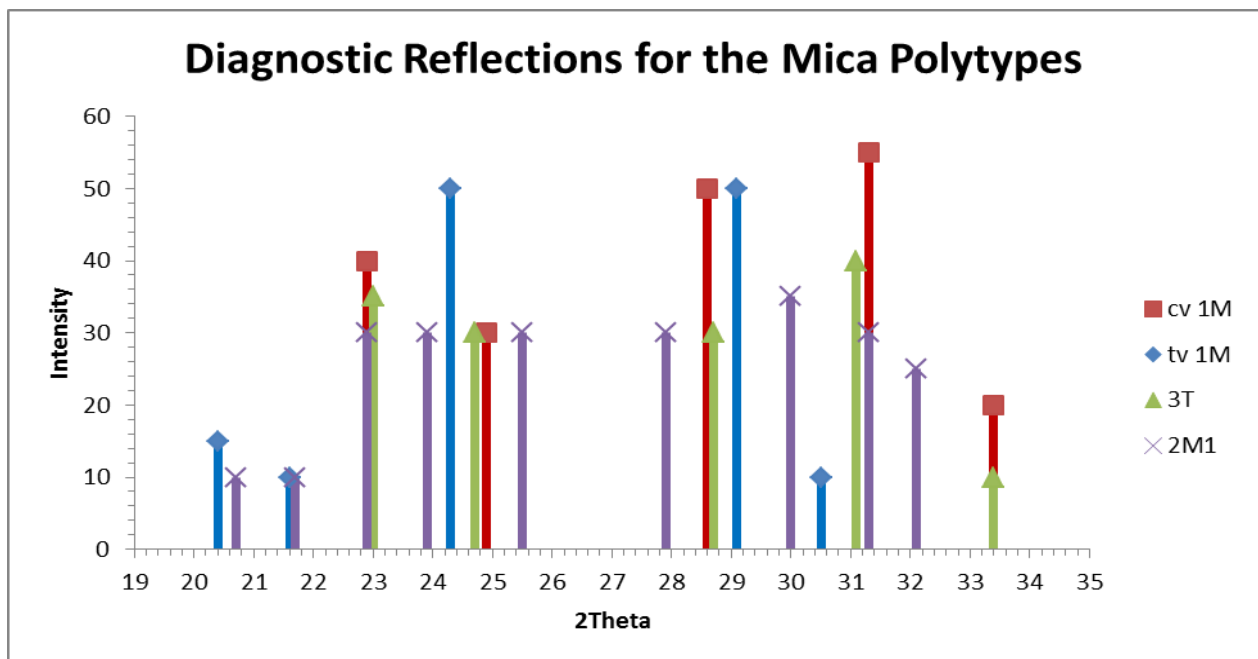


**Figure 7:** Modeled polytype intensities and their relative positions and angles.

Once the ratio of authigenic to detrital illite is determined by measuring polytypes in the XRD, the illite samples are dated by  $^{40}\text{Ar}/^{39}\text{Ar}$  step-heating thermochronology. The potassium in illite undergoes radioactive decay to argon over time and isotope dating is used to find when the authigenic illite was formed. To do this, the sample is split into three fractions based on grain size and each fraction is analyzed for polytype proportions. The three size fractions are plotted in a line based on  $^{40}\text{Ar}/^{39}\text{Ar}$  age against percent detrital illite (Fig. 8). The line of best fit is extrapolated to the point when the detrital percentage is zero, indicating the pure authigenic age, or the age of the most recent clay-forming fault movement. For our study, we analyzed the polytype ratios at Vassar College but the argon dating and thermochronology will be performed by colleagues at the University of Michigan.

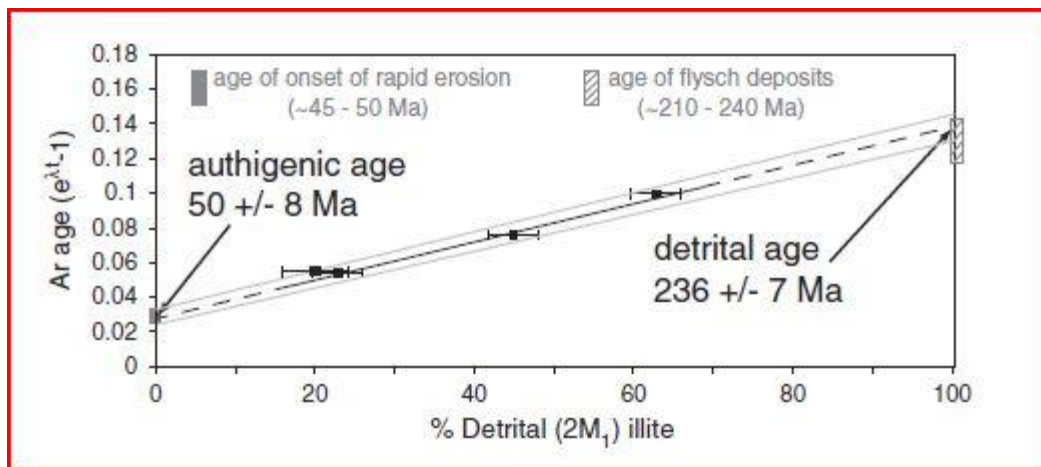


**Figure 8:** Duvall et al., 2011's plot of  $^{40}\text{Ar}/^{39}\text{Ar}$  age and detrital percentage.

## Methods

### *Sample collection*

Samples were collected from a thrust fault just outside the village of Rosendale (Figs. 1 and 2). The samples were gathered by an outside research team and given to our lab at Vassar. Four samples were collected, referred to as A, B, C, and D. Each sample was gathered from the fault gouge. Sample A was collected 1-2 cm deep into the gouge, and each subsequent sample was collected by digging deeper into the fault gouge. Sample D, the deepest, was collected at 10 cm into the fault gouge. Approximately 100 grams of each sample was placed in a sealed plastic bag.



**Figure 9:** Samples A - D were collected in the fault gouge sampling horizon. A was closest to the edge, while D was furthest into the gouge (closer to the pen).

### *Clay separation*

After a review of the literature, summarized in Table 1, three grain size fractions were selected for study: 2.6  $\mu\text{m}$  to 0.6  $\mu\text{m}$  of equivalent spherical diameter (esd), 0.6  $\mu\text{m}$  to 0.1  $\mu\text{m}$

esd, and less than 0.1  $\mu\text{m}$  esd, spanning two orders of magnitude in grain size. It is assumed that the coarser the grain size, the higher the percentage of detrital illite (Duvall et. al, 2011; Haines and van der Pluijm, 2008; Pevear, 1999; Rahl et. al., 2011). The three size fractions were used to define a line on an  $^{40}\text{Ar}/^{39}\text{Ar}$  plot that is extrapolated to estimate the detrital-authigenic age of micas in the sample. Samples C and D were separated into the three fractions. Each size fraction needs to contain roughly 20 mg.

Paper	Grain size:		
	coarse	medium	fine
Rahl, et al., 2011	2 - 0.4 $\mu\text{m}$	0.4 - 0.05 $\mu\text{m}$	<0.05 $\mu\text{m}$
Duvall et al., 2011	2 - 0.2 $\mu\text{m}$	0.2 - 0.05 $\mu\text{m}$	<0.05 $\mu\text{m}$
Pevear, 1999	2 - 0.2 $\mu\text{m}$	0.2-0.02 $\mu\text{m}$	<0.02 $\mu\text{m}$
Haines & van der Pluijm, 2008	2 - 1 $\mu\text{m}$	1 - 0.5 $\mu\text{m}$ , 0.5 - 0.1 $\mu\text{m}$ , 0.1 -0.05 $\mu\text{m}$	<0.05 $\mu\text{m}$
Verdel et al., 2011	4 – 2 $\mu\text{m}$	2 – 0.75 $\mu\text{m}$ , 0.75 – 0.2 $\mu\text{m}$	<0.2 $\mu\text{m}$ , <0.05 $\mu\text{m}$
Donohue and Walker, 2013	2.6 – 0.6 $\mu\text{m}$	0.6 - 0.1 $\mu\text{m}$	<0.1 $\mu\text{m}$

**Table 1:** This table displays the size fractions selected for this study as well as those that were taken into account when determining the size fractions for this study.

The clay size fractions were separated using Stokes' Law. Stokes' Law can be used to calculate the settling velocity of particles in water based on friction and drag on different sized particles; larger particles settle out more quickly than smaller particles (Haines and van der Pluijm, 2008). Two centrifuges were used to speed up the settling of the clays (Duvall et. al., 2011). One centrifuge (Beckman Model TJ-6) was used to separate the larger two fractions, and the other, (IEC Centra CL2) a faster centrifuge, was used to separate the smallest size fraction.

A few grams of the sample were ground with a Cole Palmer Model 4301-00 analytical mill. The ground sample was suspended in water and exposed to a sonifier (Branson Sonifier

250) for roughly two minutes. This assured that all size fractions were dispersed in suspension. The suspended sample was run through the Beckman Model TJ-6 centrifuge at a speed of 500 rpm for 4.7 minutes to settle out anything larger than 2.6  $\mu\text{m}$ . Additionally, to ensure that all of the clay size fraction was separated and in suspension, the remaining sample at the bottom of the centrifuge tube was re-sonified in combination with the remaining original ground sample and again run through the centrifuge. The total remaining suspended sample was then collected in a large beaker and placed in a 100°C oven (Fisher Scientific Isotemp 500 Series) until the water evaporated and only the clay remained. The < 2.6  $\mu\text{m}$  fraction was sonified and run through the centrifuge again at a speed of 2000 rpm for 4.3 minutes, settling out anything less than 0.6  $\mu\text{m}$ . The sample which remained in the bottom of the centrifuge tube was the 2.6 – 0.6  $\mu\text{m}$  size fraction. It was collected, dried, and readied for XRD analysis. The sample remaining in suspension was sonified and run through the IEC Centra CL2 centrifuge at a speed of 4000 rpm for 30 minutes, to separate the less than 0.1  $\mu\text{m}$  size fraction. The sample remaining in the bottom of the centrifuge tube was the 0.6 – 0.1  $\mu\text{m}$  size fraction and the sample in suspension was the less than 0.1  $\mu\text{m}$  size fraction. Both were dried and prepared for XRD analysis. These steps were only carried out on samples C and D, the samples that were collected from the deepest area of the fault gouge and thus most protected from weathering.

### *XRD Analysis*

XRD analysis was run with a Bruker AXS D2 Phaser X-ray Diffractor. For samples A – D, a glycolated wet mount sample was also prepared as to study the composition of the sample as a whole. This gave a better idea of the illite – smectite relationship in the sample. To do this, a ground portion of the <2.6  $\mu\text{m}$  sample (all size fractions) was suspended in water and run

through a filter paper. The filter peel was then applied to a slide and dried. Each slide was air dried and run after exposure to ethylene glycol for 24 hours at 60° C during which time the smectite structure expands from 15 angstroms to 16.9 angstroms. The glycolated slides were step scanned from 2 – 35 2 $\theta$  with a 0.1° step size at 4 seconds per step. The air dry and glycol analyses are used to check the mineralogy of the clay fraction of the sample and for determining the percent smectite and illite in order to evaluate the amount of weathering experienced by each sample.

For the C and D samples, random powder mounts of each size fraction were analyzed. The powder removed out of the beaker after drying was left in small, randomly formed aggregates. To achieve maximum randomness, the powder sample was allowed to distribute itself in the well mount until it was level. The accumulated powder was poured over a plastic well mount and leveled across the top of the mount using a spatula. The powder mounts were step scanned from 19 – 44 2 $\theta$  at 0.05° step size at 16 seconds per step (for C) and 40 seconds per step (for D) (Duvall et. al., 2011).

### *WILDFIRE Modeling*

To bring measured XRD data from the Bruker AXS instrument into WILDFIRE software in order to make comparisons, XRD data files first needed to be converted to comma delimited format (.csv) so that WILDFIRE could read them. By comparing and matching the peaks from the gathered data against the peaks from the modeled polytype data, the peaks that matched up in both indicated the presence of that polytype. Each polytype or non-illite (chlorite and calcite) peak could also be identified and evaluated.

WILDFIRE modeling software (Rahl et al., 2011; Duvall et al., 2011; Haines and van der Pluijm, 2008) was used to compare the XRD plots and to determine the randomness of the XRD mount and the ratio of authigenic (1M and 1M<sub>d</sub>) and detrital (2M<sub>1</sub>) polytypes. Multiple initial parameters were transferrable from the XRD software. The range was 19 – 44 2 $\Theta$  and the step size was 0.05°, for example. WILDFIRE software was used to determine the Dollase Factor (D) of each sample. The Dollase Factor is a measure of the degree of random orientation of the powder mount. Possible values ranged from 0.5 to 1, where 0.5 represents the least random orientation of grains and a value of 1 represents a perfectly random mount. By adjusting the Dollase Factor when modeling and comparing the outputs with the measured XRD plots, the degree of randomness in the mount could be determined.

WILDFIRE software was used to determine the amount of disorder in the sample (D). The amount of disorder in 1M polytypes is modeled using the “probability of zero rotation” factor (P<sub>0</sub>) which ranged from 1/3 to 1 and represents the degree of disorder or, conversely, TOT layer alignment in the models. A P<sub>0</sub> value of 1/3 represents the most disorder possible, while a value of 1 corresponds to no disorder. Through varying the P<sub>0</sub> and comparing the outputs with the measured plots, the amount of disorder in the measured samples could be approximated.

Once the D and P<sub>0</sub> values were approximated, they were incorporated into final polytype models of 1M/1M<sub>d</sub> and 2M<sub>1</sub>. These models were mixed to create an ideal model for the measured XRD output. The polytype models were added together using a sliding scale of ratios which added to peak intensity of one polytype model while decreasing the other. The ratios were altered until the result reflected the measured XRD data, at which point the ratio was recorded.

This process was performed on each of the three size fractions (2.6 – 0.6  $\mu\text{m}$ , 0.6 – 0.1  $\mu\text{m}$ , and < 0.1  $\mu\text{m}$ ) of sample D.

## Results

### *Smectite*

The first results gathered were those of the air dried and glycolated XRD runs of samples A-D. These plots were measured to determine the amount of smectite present in each sample. Smectite is indicative of weathering in the sample and would give a better idea of which samples to focus on. Glycolated smectite has a peak at 16.9 Å (around  $5^\circ 2\Theta$ ). Figure 10 shows the plots of the A, B, C, and D glycolated samples, there is another peak (possibly a chlorite – 14.2 Å or illite – 9.98 Å peak) that begins at  $6^\circ 2\Theta$ , so the smaller smectite peak is cut short. A smectite peak can be seen in samples A and B. In sample C there is a nearly indiscernible rise around  $5^\circ 2\Theta$  which is possibly indicative of smectite. In sample D, however, no smectite is visible. Therefore, sample D was chosen for further study because of minimal weathering.

### *WILDFIRE Parameters*

XRD analysis of the random powder mounts from the three size fractions of sample D can be seen in Figure 11. The process of developing the models to compare to the measured XRD plots of each size fraction included determining the amount of disorder of the 1M polytype and estimating the degree of randomness in the mounts. Ultimately, the results showed that there was minimal disorder in the clay structure. When comparing the  $P_0$  values in the range of 1/3 to 1 (Fig. 12), a value of 1 demonstrated the best fit to the measured plot. Therefore, the model

reflected that the sample had an almost perfect alignment of TOT layers, or minimal disorder. Alteration of  $P_0$  affected the intensity of the polytype specific peaks and how they modulate above the background of the plot: the less disorder there was, the more intense the peaks were in their rise above the background. This was the case in the measurement of the sample, especially compared to the more disordered options. If there was any disorder in the sample, it was minimal.

The other factor accounted for in modeling, the degree of randomness of the mounts, was determined by the Dollase Factor. Dollase value possibilities ranged from 0.5 (ordered) to 1 (perfectly random) (Fig. 13). Creating a more randomly oriented mount ensures better accuracy in results. In a perfectly random mount (Dollase Factor of 1), the polytype specific peaks are intensified. A Dollase value of 0.7 was found to be most accurate for sample D mounts, meaning that the mounts created could have been more random. In order to ensure this in the future, an end-packer device as referenced in Duvall et al., 2011 or an Al sample holder described in Haines and van der Pluijm, 2008 could be used to create powder mounts.

To ensure that peak width and sharpness was representative in models, the mean defect-free distance ( $\delta$ ) and maximum diffracting domain size ( $N_3$ ) were modified to reflect full width half maximum (FWHM) values for each size fraction's 003 illite peak. Mean and maximum defect-free distances refer to the number of TOT layers that consecutively align along C in a parallel fashion. Mean defect-free distance is the average number of layers in a different domain whereas maximum defect-free distance is the maximum number of that layers in a domain. Typically, the value of  $N_3$  will be five times the value of  $\delta$  (Moore and Reynolds, 1997). Using NEWMOD modeling software, the FWHM values were calculated for the 003 illite peak in each

size fraction. For the 2.6-0.6  $\mu\text{m}$ , 0.6-0.1  $\mu\text{m}$ , and  $<0.1$   $\mu\text{m}$  size fractions, the FWHM values were  $0.302^\circ$ ,  $0.490^\circ$ , and  $0.521^\circ$ , respectively. To match these values,  $\delta$  and N3 were altered. The two end member size fractions (2.6-0.6  $\mu\text{m}$  and  $<0.1$   $\mu\text{m}$ ) were best represented by  $\delta$  values of 11.3 and 7.5, respectively, and N3 values of 50 and 25, respectively. These values were then transferred to the WILDFIRE models. It is important to note that the N3 values were capped by the program (at 25 and 50, depending on which solution of the software being used), limiting possible  $\delta$  values.

### *Non-micaceous Minerals*

The final results included comparisons of the combinations of both polytype models to the measured results. By combining the 1M model and the  $2M_1$  model on a ratio-based scale, percentages of each polytype could be determined (Fig. 14). While performing calculation, it should be noted that non-mica peaks were identified among the polytype peaks, often drowning them out. Chlorite was present in all three size fractions, with major peaks appearing around  $25$  and  $31^\circ 2\theta$  at intensities high enough to drown out possible polytype peaks in those locations. Additionally, a cluster of two chlorite peaks around  $34-35^\circ 2\theta$  may have altered the appearance of mica polytype peaks there. A calcite peak was also found in the 2.6-0.6  $\mu\text{m}$  and  $<0.1$  size fractions between  $29^\circ$  and  $30^\circ 2\theta$  at high enough intensities to interfere with mica polytype peaks there. Chlorite was modeled as a separate plot and added to both polytype models so that the combined effect of the chlorite peaks could be factored into the final model (Fig. 15). Calcite, however, could not be modeled by WILDFIRE since it is not a clay mineral.

## Polytype Percentages

When a relative proportion of the two final models best matched the measured plot of each size fraction, the ratio was recorded and calculated into a percentage. For the largest size fraction, 2.6-0.6  $\mu\text{m}$ , the polytype percentage was 33.33% 1M and 66.66% 2M<sub>1</sub> (Fig. 16). For the 0.6-0.1  $\mu\text{m}$  size fraction, the polytype percentage was 50% 1M and 50% 2M<sub>1</sub> (Fig. 17). And for the <0.1  $\mu\text{m}$  size fraction, the polytype percentage was 77.77% 1M and 22.22% 2M<sub>1</sub> (Fig. 18).

## Results (Figures)

### Commander Sample ID (Coupled TwoTheta/Theta)

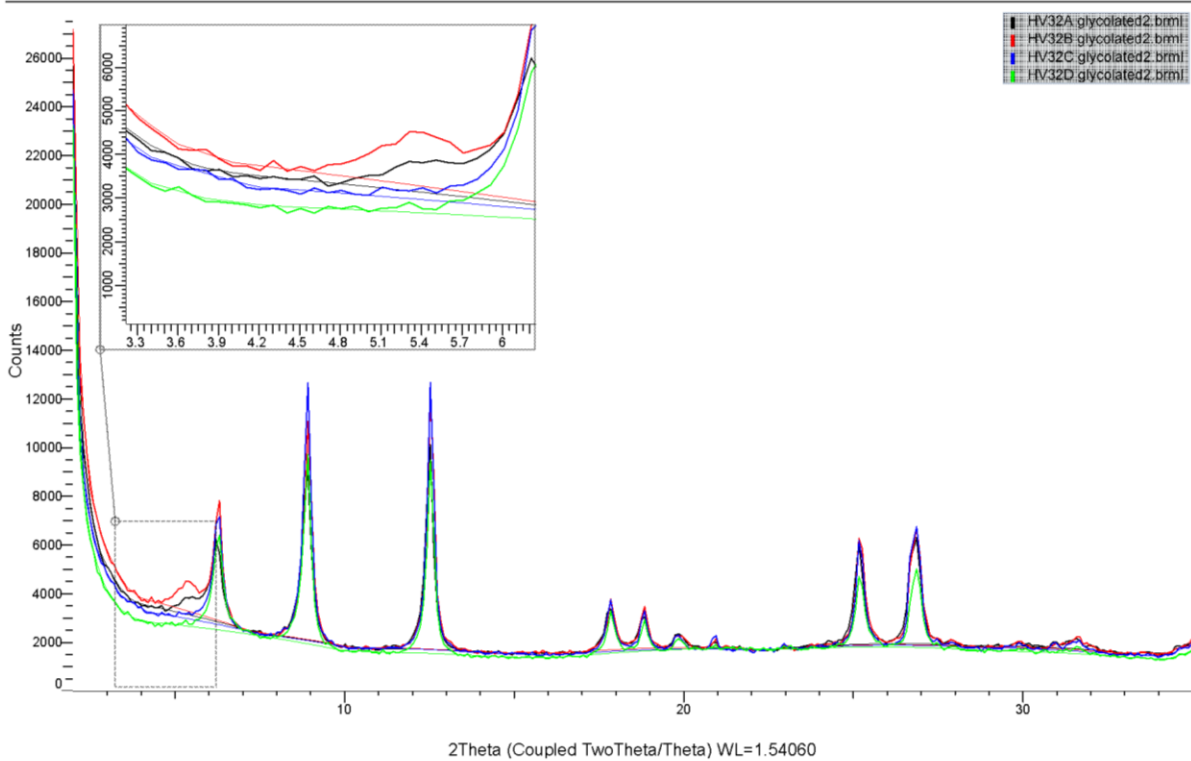


**Figure 10:** The glycolated samples (A: black, B: red, C: blue, D: green) with a zoomed view of the expanded smectite peak (at 5 2 $\Theta$ ).

### Commander Sample ID (Coupled TwoTheta/Theta)

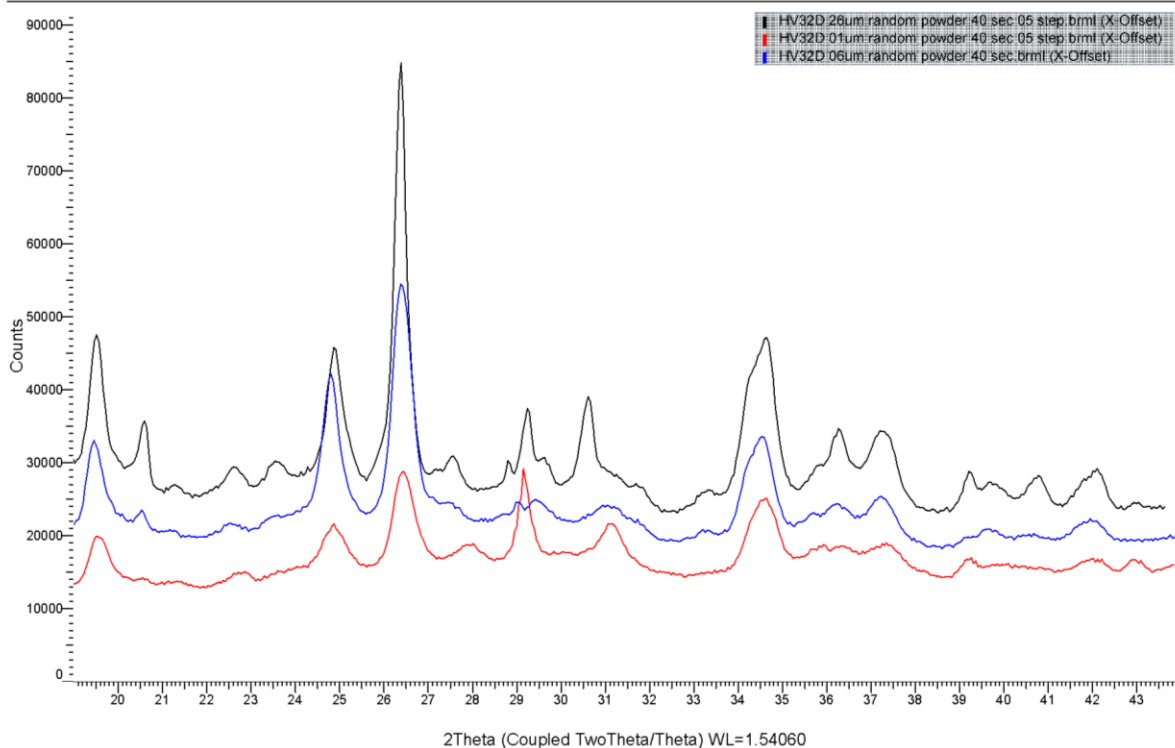


**Figure 11:** The three size fractions of sample D (2.6-0.6 μm: black, 0.6-0.1 μm: blue, <0.1 μm: red) overlain on one another.

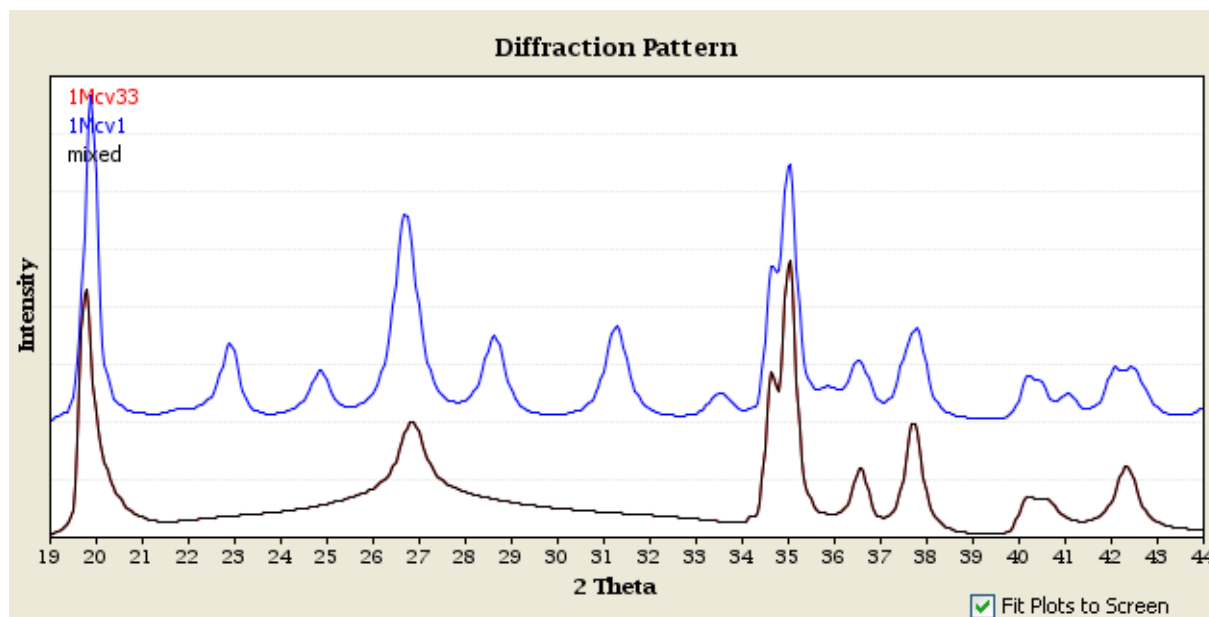


**Figure 12:** Both ends of the range of  $P_0$  values: 1/3 (black) to 1 (blue).  $P_0 = 1$  displays more definitive polytype peaks.

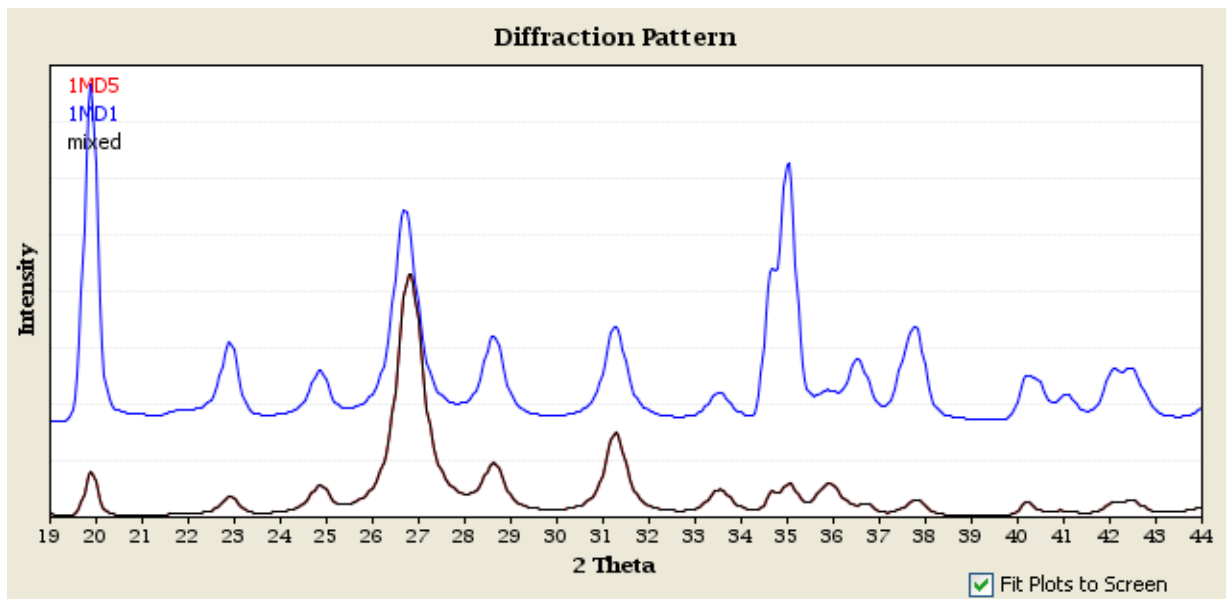


**Figure 13:** Both ends of the range of Dollase values: 0.5 (black) to 1 (blue).  $D = 1$  (perfectly random) displays more definitive polytype peaks.

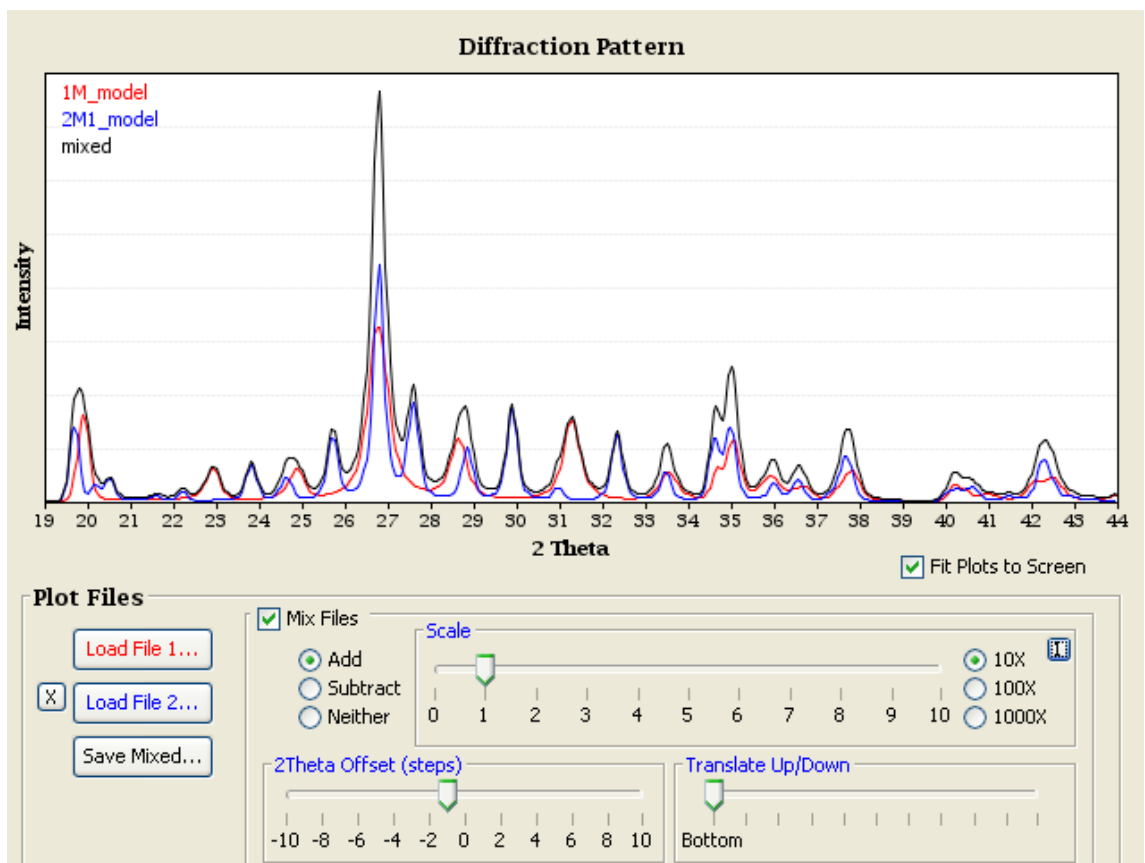


**Figure 14:** The red plot is the modeled 1M, the blue plot is the modeled  $2M_1$ , and the black plot is the combination of the intensities of both. The scale of 1 represents 50/50 percentage between 1M/ $2M_1$ .

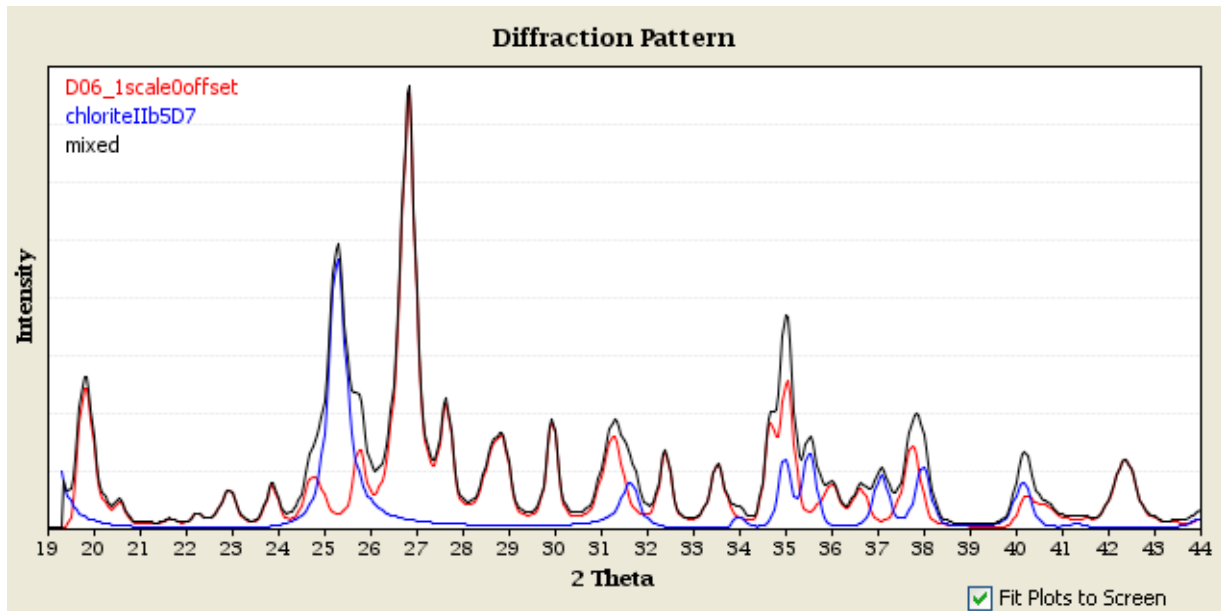


**Figure 15:** The red plot is the modeled 1M/2M<sub>1</sub> combination from Fig. 14, the blue plot is modeled chlorite, and the black plot is the combination of the intensities of both, displaying a more ideal final model.

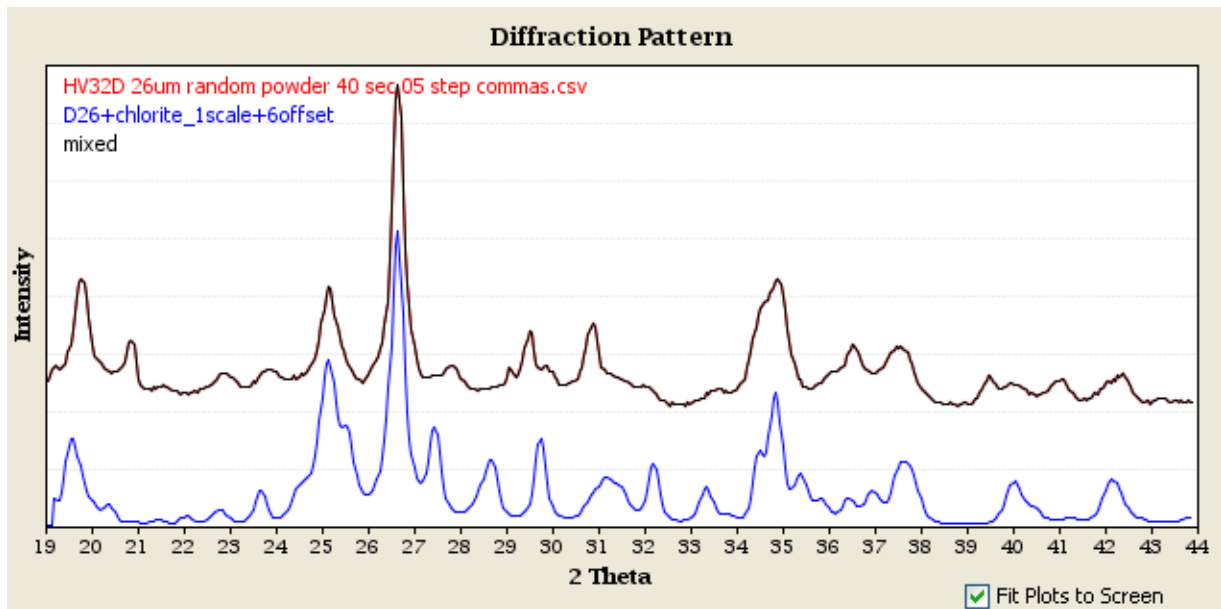


**Figure 16:** The blue plot is the final modeled 1M/2M<sub>1</sub> combination with chlorite accounted for and the black plot is the measured 2.6-0.6 μm size fraction for comparison.

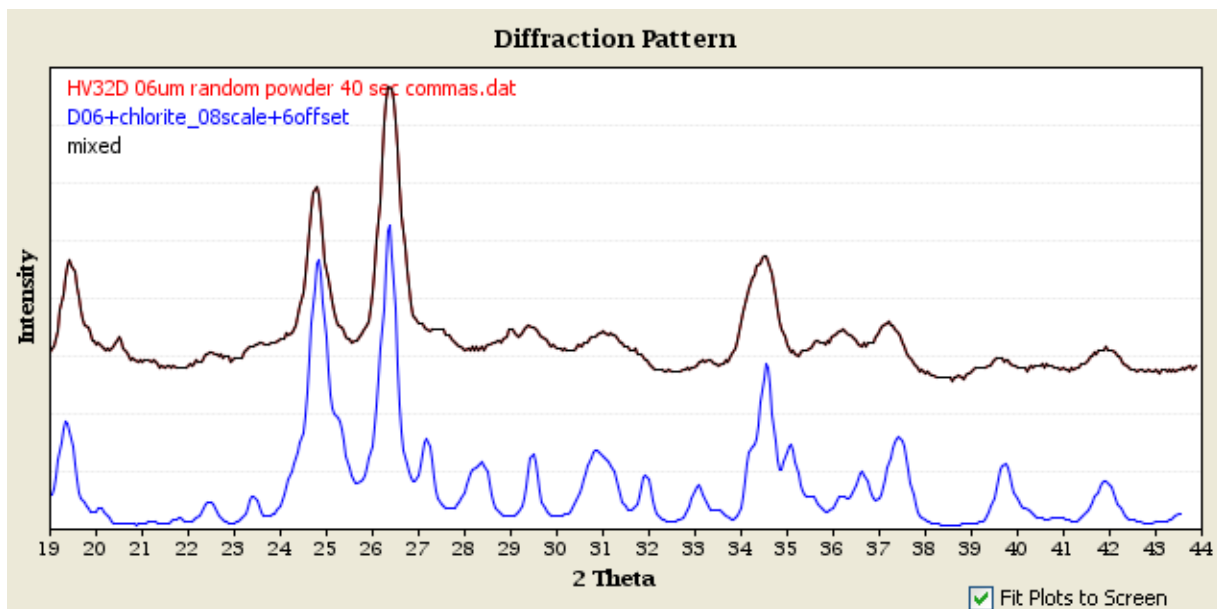


**Figure 17:** The blue plot is the final modeled 1M/2M<sub>1</sub> combination with chlorite accounted for and the black plot is the measured 0.6-0.1 μm size fraction for comparison.

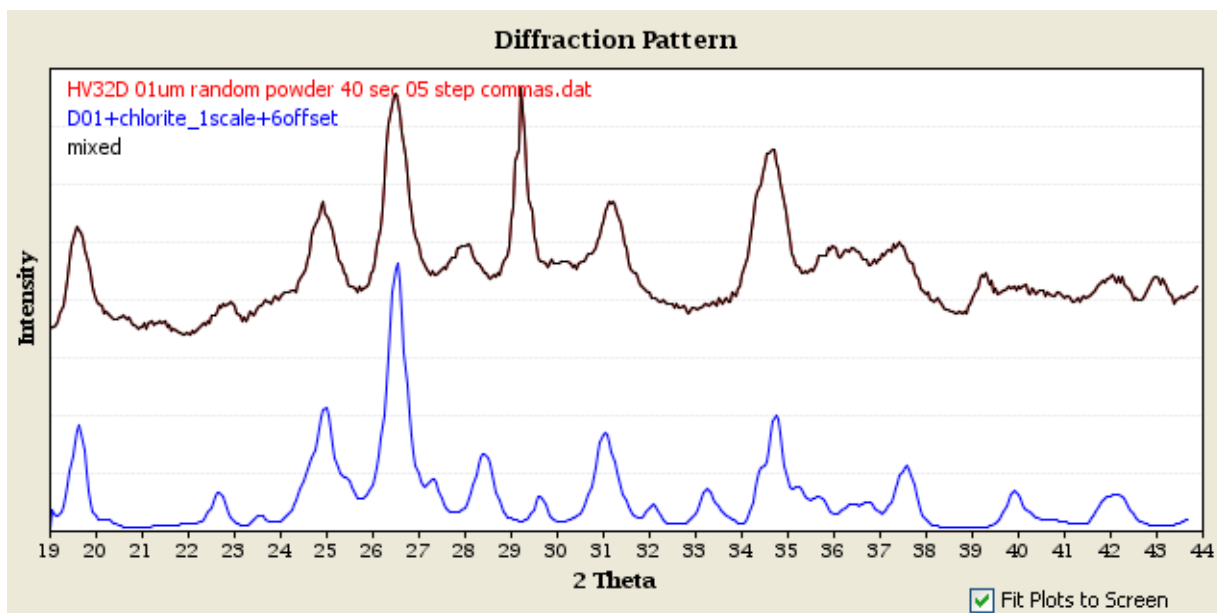


**Figure 18:** The blue plot is the final modeled 1M/2M<sub>1</sub> combination with chlorite accounted for and the black plot is the measured <0.1 μm size fraction for comparison.

## Discussion

### *Smectite*

By comparing the intensity of smectite peaks in each of the glycolated plots (Fig. 10), it appears that A and B have significant amounts of weathering while in C and D weathering was minimal. Bearing these results in mind, samples C and D were split into size fractions and D was selected to be analyzed further. The presence of smectite indicates that the mineralogical reaction caused by weathering and resulting in the transition of illite to smectite had begun (Larson et al., 2009). It is to be expected that A and B would have the highest amounts of smectite, as they are closest to the weathered edge of the fault gouge (Fig. 9). Samples C and D were more protected from the elements, and thus preserve the authigenic illite presumably formed when the fault occurred.

### *Disorder*

The results of the WILDFIRE modeling indicated that there was no significant rotational disorder in the illite sampled from the Rosendale fault gouge (Fig. 12). This result was surprising given the literature review. Each paper reviewed that set up an experiment similar to this one (Rahl et al., 2011; Haines and van der Pluijm, 2008; Duvall et. al., 2011) got results that included a disordered fraction to the 1M polytype. The majority of faults in these previous studies, however, are around 200 million years old or younger. The hypothesized age of the Rosendale fault is closer to 375-260 million years, nearly twice as old as the oldest fault studied in the reviewed papers. In the hundreds of millions of years between when the Rosendale fault formed and when those faults formed, it is possible that the majority of disorder in the illite could be

annealed through kinetics, depending on the temperature at which the rocks were held. The disorderly rotation of TOT layers may have been able to slowly align over time (Moore and Reynolds, 1997). Another possibility, however, is that during the 24 hours of heating to 100° C each sample underwent as it was in suspension after being run through the centrifuge, the illite may have annealed, removing all disorder.

### *Polytypes*

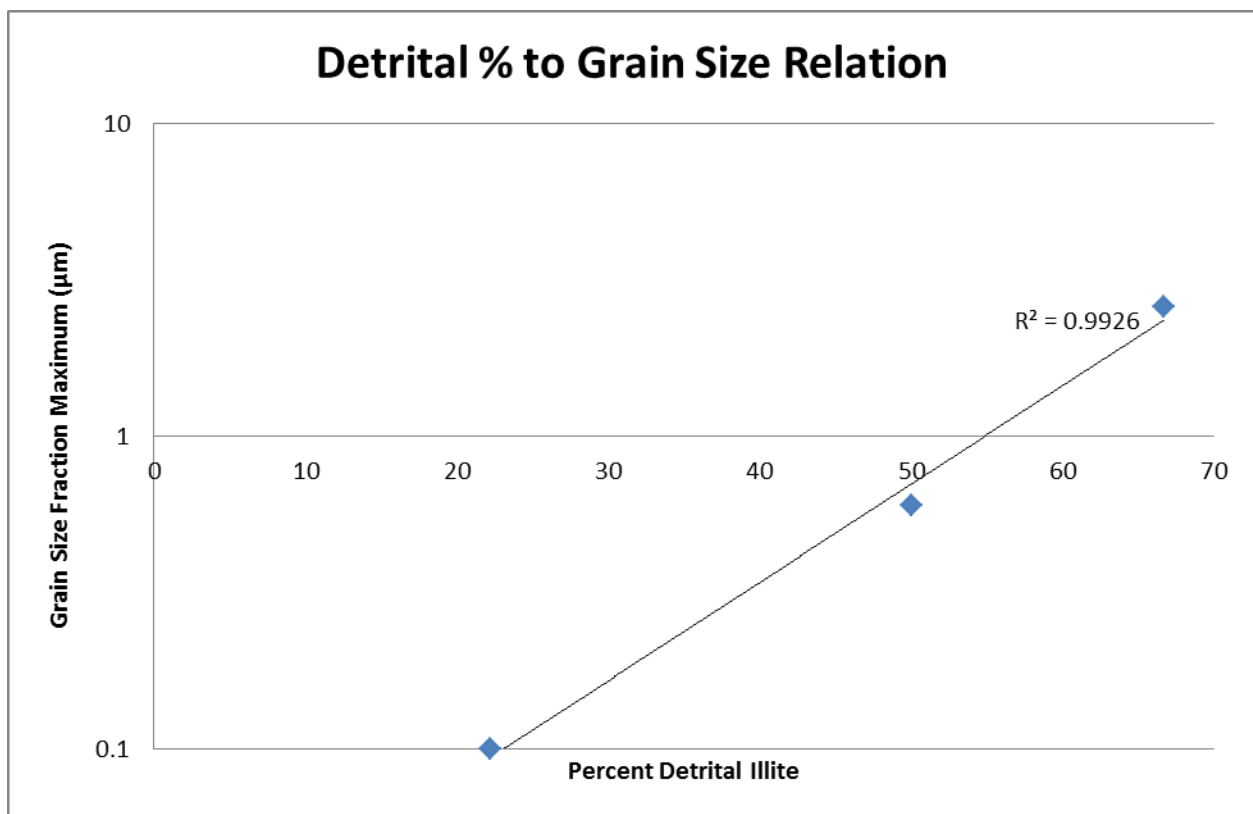


**Figure 19:** The relation between the % detrital (2M1) illite and grain size on a logarithmic scale.

Figure 19 demonstrates the positive linear relationship between grain size and the detrital (2M<sub>1</sub>) component of each grain size. With an  $R^2$  value of 0.9926, the points line up nearly perfectly. Although the grain size axis is logarithmic, the fact that each of the size fractions is a

full order of magnitude apart justifies it. The linear representation validates the idea that the polytype percentages of the two end member fractions were calculated accurately. Each size fraction's polytype percentage was calculated independently and the results supported the initial hypothesis that each smaller fraction would have less and less detrital illite. Since larger grains can be assumed to be older to have enough time to grow larger, it can be assumed that they have a higher detrital percentage once the samples are dated. Using three size fractions, the trendline can be extended until it hypothetically represents 100% authigenic illite, indicating the moment the fault began, when graphed against  $^{40}\text{Ar}/^{39}\text{Ar}$  dating (Haines et al, 2011; Duvall et al., 2011).

The detrital illite, of the  $2M_1$  polytype, comes from the wall rock and has a uniform age from well before the fault was formed. The authigenic illite of the  $1M$  polytype was formed throughout the period of time that the fault was most recently active, and thus can at best offer a date of the most recent fault activity. Regardless, we know that whenever the authigenic illite appears, that the fault is active. By extrapolating the relationship between  $^{40}\text{Ar}/^{39}\text{Ar}$  and the percentage of detrital illite in each size fraction, the  $^{40}\text{Ar}/^{39}\text{Ar}$  radiometric analysis can accurately date the time of the fault by predicting at what time the sample formed if it was made up of 100% authigenic illite, meaning authigenesis was under way and the fault was active.

Vassar College, the site of this clay polytype research, does not have an accelerator mass spectrometry (AMS) system, but will send the separated size fraction samples to the University of Michigan along with this analysis of polytypes and detrital/authigenic percentages. There, the exact date of the most recent movement on the Rosendale fault will be determined.

## Bibliography

- Burmeister, Kurtis C., and Stephen Marshak. "Along-strike changes in fold-thrust belt architecture: Examples from Hudson Valley, New York." *Geological Society of America Field Guide* 8 (2006): 199-216. Print.
- Duvall, Alison R., Martin K. Clark, Ben A. van der Pluijm, and Chuanyou Li. "Direct dating of Eocene reverse faulting in northeastern Tibet using Ar-dating of fault clays and low-temperature thermochronometry." *Earth and Planetary Science Letters* 304 (2011): 520-526. Print.
- Haines, Samuel H.. "Fault thrust ages from the South-Central Pyrenees fold-and-thrust belt - Demonstration of in-sequence thrusting and the geological significance of wall-rock provenance ages extrapolated from gouge-dating." *Geological Society of America Bulletin* 41.7 (2009): 479. Print.
- Larson, Bruno, Boris A. Sakharov, Francis Claret, and Victor A. Drits. "Diagenetic smectite-to-illite transition in clay-rich sediments: A reappraisal of X-ray diffraction results using the multi-specimen method." *American Journal of Science* 309.6 (2009): 476-516. Print.
- Marshak, Stephen. "Structural geology of Silurian and Devonian strata in the Mid-Hudson Valley, New York: Fold-thrust belt tectonics in miniature." *Geological Survey* 41 (1990): 1-66. Print.
- Moore, Duane Milton, and Robert C. Reynolds. *X-ray Diffraction and the Identification and Analysis of Clay Minerals*. 2nd ed. Oxford: Oxford University Press, 1997. Print.
- Pevear, David R.. "Illite and hydrocarbon exploration." *National academy of Sciences* 96 (1998): 3440-3446. Print.

Rahl, Jeffrey M., Samuel H. Haines, and Ben A. van der Pluijm. "Links between orogenic wedge deformation and erosional exhumation: Evidence from illite age analysis of fault rock and detrital thermochronology of syn-tectonic conglomerates in the Spanish Pyrenees." *Earth and Planetary Science Letters* 307 (2011): 180-190. Print.

Verdel, Charles, Nathan Niemi, and Ben A. van der Pluijm. "Thermochronology of the Salt Spring fault: Constraints on the evolution of the South Virgin - White Hills detachment system, Nevada and Arizona, USA." *Geological Society of America Bulletin* 7.3 (2011): 774-784. Print.